

NUSC Technical Document 8523
5 May 1989

2

Computational Corrosion Analysis for Design of Microelectronic Components Under Conditions of Atmospheric Corrosion

Presented at CORROSION/88,
National Association of Corrosion Engineers
Annual Conference, 21-25 March 1988,
St. Louis, Missouri

AD-A209 346

Raymond S. Munn
Engineering & Technical Support Department



SDTICD
ELECTE
JUN 16 1989
H

Naval Underwater Systems Center
Newport, Rhode Island / New London, Connecticut

Approved for public release; distribution is unlimited.

89 6 16 326

PREFACE

This document was prepared in support of the AN/BSY(2) Design Assurance Program under NUSC Project No. A45333, T. G. Bucko, Principal Investigator.

REVIEWED AND APPROVED: 5 May 1989

A handwritten signature in cursive script, appearing to read "Russell L. Brown".

R. L. BROWN
HEAD: ENGINEERING AND TECHNICAL
SUPPORT DEPARTMENT

REPORT DOCUMENTATION PAGE

1a. REPORT SECURITY CLASSIFICATION UNCLASSIFIED		1b. RESTRICTIVE MARKINGS	
2a. SECURITY CLASSIFICATION AUTHORITY		3. DISTRIBUTION / AVAILABILITY OF REPORT Approved for public release; distribution unlimited.	
2b. DECLASSIFICATION / DOWNGRADING SCHEDULE			
4. PERFORMING ORGANIZATION REPORT NUMBER(S) NUSC TD 8523		5. MONITORING ORGANIZATION REPORT NUMBER(S)	
6a. NAME OF PERFORMING ORGANIZATION Naval Underwater Systems Center	6b. OFFICE SYMBOL (If applicable) 44	7a. NAME OF MONITORING ORGANIZATION	
6c. ADDRESS (City, State, and ZIP Code) New London Laboratory New London, CT 06320		7b. ADDRESS (City, State, and ZIP Code)	
8a. NAME OF FUNDING / SPONSORING ORGANIZATION	8b. OFFICE SYMBOL (If applicable)	9. PROCUREMENT INSTRUMENT IDENTIFICATION NUMBER	
8c. ADDRESS (City, State, and ZIP Code)		10. SOURCE OF FUNDING NUMBERS	
		PROGRAM ELEMENT NO.	PROJECT NO. 644Y00
		TASK NO.	WORK UNIT ACCESSION NO.
11. TITLE (Include Security Classification) COMPUTATIONAL CORROSION ANALYSIS FOR DESIGN OF MICROELECTRONIC COMPONENTS UNDER CONDITIONS OF ATMOSPHERIC CORROSION			
12. PERSONAL AUTHOR(S) Raymond S. Munn			
13a. TYPE OF REPORT Summary	13b. TIME COVERED FROM _____ TO _____	14. DATE OF REPORT (Year, Month, Day) 1989 May 5	15. PAGE COUNT 18
16. SUPPLEMENTARY NOTATION Presented at CORROSION/88, National Association of Corrosion Engineers Annual Conference, 21-25 March 1988, St. Louis, Missouri			
17. COSATI CODES		18. SUBJECT TERMS (Continue on reverse if necessary and identify by block number)	
FIELD	GROUP	Computational Corrosion Analysis; Corrosion; Electronic Packing; Electronic Components; Finite Element Analysis; (x)	
19. ABSTRACT (Continue on reverse if necessary and identify by block number) Numerical corrosion analysis capability is extended to applications of thin electrolytes (atmospheric condensates) on multimetallic and multipotential electronic components. Dissolution or electrodeposition rates are predicted for the metal components on printed wiring boards. Guidelines for printed wiring board spatial design are projected from the results of these analyses. <i>Keywords:</i>			
20. DISTRIBUTION / AVAILABILITY OF ABSTRACT <input type="checkbox"/> UNCLASSIFIED/UNLIMITED <input checked="" type="checkbox"/> SAME AS RPT. <input type="checkbox"/> DTIC USERS		21. ABSTRACT SECURITY CLASSIFICATION UNCLASSIFIED	
22a. NAME OF RESPONSIBLE INDIVIDUAL Raymond S. Munn		22b. TELEPHONE (Include Area Code) (203) 440-4972	22c. OFFICE SYMBOL 44

TABLE OF CONTENTS

	Page
LIST OF ILLUSTRATIONS	ii
LIST OF TABLES	ii
INTRODUCTION	1
PROBLEM.	1
ANALYSIS	2
RESULTS.	3
DISCUSSION OF RESULTS.	4
CONCLUSIONS.	6
REFERENCES	17

Accession For	
NTIS GRA&I	<input checked="" type="checkbox"/>
DTIC TAB	<input type="checkbox"/>
Unannounced	<input type="checkbox"/>
Justification	
By _____	
Distribution/	
Availability Codes	
Dist	Avail and/or Special
A-1	



LIST OF ILLUSTRATIONS

Figure		Page
1	Conditions for Atmospheric Corrosion	7
2	A. Geometry of Electrolyte Section B. Finite Element Model of Electrolyte	8
3	A. Polarization Curve for Copper in Seawater Condensate Electrolyte B. Polarized Copper Electrodes in Seawater Condensate Electrolyte	9
4	Nearfield Distribution of Electrochemical Potential in Electrolyte.	10
5	A. Case 1D Potential Distribution Over PWB Surface.	11
	B. Case 1D Current Density Distribution Over PWB Surface. . .	12

LIST OF TABLES

1	Printed Wiring Board Analysis Cases	13
2	Potential Results for Analysis Cases.	14
3	Current Density Results of Analysis Cases	15

COMPUTATIONAL CORROSION ANALYSIS FOR DESIGN OF MICROELECTRONIC COMPONENTS UNDER CONDITIONS OF ATMOSPHERIC CORROSION

INTRODUCTION

To perform its assigned mission, the Navy has been heavily involved with the use of electronics components in marine environments, shipboard and outboard, to a degree increasing with emergent technology. This involvement has been accompanied by significant challenges of electronics failures that can limit accomplishment of missions dependent on these components.

Electronics components can fail due to a number of mechanical, material, environmental, design, or manufacturing reasons. It has been verified, however, that about 20% of electronics failures are caused by corrosion.¹ Corrosion in electronics components can have any of several different causes stemming from design, manufacture, or use. This technical document will address only the design-related causes of galvanic corrosion and electrodeposition that may be attributed to juxtaposition of dissimilar metals or of similar metals with different circuit potentials.

Specifically, this document will demonstrate the application of numerical corrosion analysis methods to mitigate corrosion and electrodeposition of printed wiring boards (PWB's). The overall objective of this work was to develop design guidelines that would improve the operability and reliability of shipboard electronics in humid environments.

PROBLEM

The PWB's of current combat system electronics experience a variety of in-service and environmental situations owing to thermal cycling, shock loading, and humid atmospheres. Temperature cycling in a humid environment provides the condensation conditions necessary for atmospheric (thin-film) corrosion of the components of the boards (figure 1) and also causes deflections sufficient to crack conformal coatings or disbond them from the solder joints. This results in corrosion of surface components and diffusion of moisture into the porous dielectric layers, allowing corrosion and electrodeposition between copper film conducting layers. *Cor 40 DD 473*

The Naval Underwater Systems Center (NUSC) supports the Naval Weapons Support Center (NWSC), which is the lead Navy laboratory for electronics modules specifications for the hardware standardization program, by monitoring progress of contractors in the copper thick-film program. The Center is, therefore, interested in quantitatively applying available corrosion theory and protection practice to PWB's. NUSC led the development of numerical corrosion analysis methods over the past decade,^{2,3,4} has applied the methods to corrosion and cathodic prediction problems,^{5,6} and most recently has applied the methods to microcorrosion phenomena of pitting⁷ and crevice corrosion⁸ under sponsorship of the Office of Naval Research (ONR).

In quantitatively applying corrosion theory, cathodic protection principles, and numerical corrosion analysis to PWB's, other factors inherent to the local nature of the phenomena must be considered. The effect of thin electrolyte was considered analytically by McCafferty⁹ to establish the threshold value of electrolyte thickness as a departure from bulk electrolyte conditions. In the current work, however, the electrolyte thickness can be much thinner, to the extent that it may no longer be isotropically conductive. The varying degree of aeration (oxygen content) throughout the area wetted by an electrolyte droplet has been known to affect corrosion, indeed being a source of galvanic corrosion itself.¹⁰ It is hypothesized that on the droplet scale or for very thin electrolytes, surface tension may be a significant factor in the kinetics of the corrosion reaction, being a high-energy region of electrolyte. The diffusion of condensed moisture into porous dielectric layer of an electronics board provides an "electrolyte" medium of ion migration between layers of conductors of unequal potentials or dissimilar materials;¹¹ this leads to metal dissolution at the relative anode and dendritic electrodeposition at the cathode, leading to an open or short circuit. These phenomena all affect PWB reliability; however, the work described by this document was limited to numerical corrosion analysis of the galvanic couple due to juxtaposition of conductive copper films with different circuit potentials.

ANALYSIS

The methods of numerical corrosion analysis developed earlier were applied to this problem. In summary, the method solves the Laplace equation for a mathematical model of the conducting electrolyte containing components of a galvanic system of wetted metals. This solution is accomplished using the finite element method (FEM), which accounts for the geometry of the electrolyte to any desired degree of accuracy. The numerical corrosion analysis method also used fully accounts for the nonlinear electrode kinetics (electrodics) of the constituent metals by analytically characterizing their measured polarization behaviors in the specific electrolyte.

In the present work, the additional capability of prescribing known differences in potential between wetted metals (herein being different circuit elements wetted by a common condensate) was added to the numerical corrosion analysis method. This is accomplished by numerically imposing a prescribed potential difference between the metals ("nodes," in the spirit of the FEM), a relative constant only that does not interfere with their electrochemical potentials, which have "absolute" values that are important relative to a standard reference electrode.

The electrolyte geometry that was used for development and demonstration in the work is shown in figure 2A. The dimensions of the electrolyte region considered are 0.1 cm wide by 0.001 cm (10 μm) thick as shown, with the third dimension being very deep relative to the others. This represents a section through a condensed electrolyte that wets two copper film conductors on an insulative board. Free or insulated surfaces exist on all but the lower boundary, which contains the alternate locations of two copper thin-film conductors and insulators. In this series of numerical experiments,

the positions of the two were varied as shown, the potential circuit bias between the two copper strips was varied between 500 mV and 1000 mV, and the electrolyte thickness was varied between 1.7 μm and the "bulk" thickness of 500 μm . The geometric variation in finite element thickness as shown in the FEM model of figure 2B was employed to account for the thin electrolyte situation.

The two copper strips were rendered relatively anodic and cathodic by the imposed potential difference of 500 mV between them, a typical value for differences in circuit potentials. This relationship is demonstrated by the polarization curve of copper in sea water electrolyte shown in figure 3A. By impressing a relative potential between the two electrodes, they assume relatively anodic and cathodic positions on the polarization curve (figure 3B). Of course, in the situations when unequal areas are exposed or the geometrical configuration provides a nonsymmetrical arrangement of the electrodes, the governing polarization curve is represented versus total applied current, in the spirit of the mixed potential theory. The FEM accounts for such geometrical considerations, such as "throwing power."

The cases analyzed in this investigation are given in table 1. The variables originally under consideration were electrolyte thickness (from condensate to bulk), electrode spacing, and electrode bias potential. Since the condition of condensation was the principal concern, this variable was fixed at the thin-film dimension (typically 0.1-10 μm). The electrode spacing was varied from a minimum of 100 μm (equal to the copper strip width) to a maximum of 300 μm , and the bias potential was varied from 500 mV (reported in reference 11 to be a threshold potential difference for dendritic electrodeposition growth of copper on copper in acid solution without added copper ions) to 1000 mV = 1V.

The numerical corrosion analyses described above were performed using the MARC Finite Element Computer Program on a VAX 11/782 supermini computer, requiring approximately 15 minutes of computational time. The FEM model took approximately one hour to construct with the MENTAT finite element pre/post processing graphics program. The processing of the copper polarization data to provide an analytical characterization of its behavior for boundary condition implementations required approximately one hour using the preprocessing segment of the GALVANALYSIS(tm) program. The graphic display of potentials over the cathode/insulator/anode surface required approximately ten minutes for each case, using the graphics program.

RESULTS

The results of the first low-conductivity ($\sigma = 1/10 \sigma_{\text{sw}}$) case (Code 1D, table 1) of two copper circuit strips of width 100 μm , separated by 100 μm , wetted by a 10 μm thick sea water condensate, and with a circuit bias of 500 mV, are shown in figure 4 as the near-field distribution of electrochemical potential. (For clarity purposes, this figure does not show the results for the entire model.) The contours in this figure depict the strong horizontal potential gradient imposed, of course, between the relative anode on the right and the relative cathode on the left. Figure 5A displays the results of this same case as a potential versus distance plot across the plane of the electrodes; figure 5B displays the applied current density along the lower surface of the electrolyte.

Table 2 gives the magnitudes of copper strip potentials and the magnitudes of maximum current density on the copper surfaces, for each of the numerical experiments described in table 1.

DISCUSSION OF RESULTS

The polarization curve for copper in sea water is shown in figure 3A, and the potential bias imposed in these experiments (varied to include 500 mV, 750 mV, and 1000 mV) is shown qualitatively in figure 3B. By means of the power supply in the circuit on the printed wiring board, the two copper electrodes of figure 2 were polarized relative to one another, one anodically (higher potential) and the other cathodically. The polarized positions on the polarization curve are determined by two constraints (1) the difference in potential between the two must be the imposed bias ($\Delta\phi$); and (2) the total applied currents on the two electrodes must be equal in magnitude but opposite in sense to enforce charge conservation in the electrolyte. In a case of equal electrode areas, the latter conditions should translate to equal current densities. However, in this case, geometry effects, although symmetric, cause spatial variations of current density (and potential) on the electrode surfaces. Hence, tables 2 and 3 report extreme values of those variables.

Figure 4 shows that the potential gradient and, thus, the current flow in the electrolyte are virtually purely horizontal between the electrodes. This effect is due to the thin dimensions of the electrolyte and the constraint of zero potential gradient normal to the top (free) surface of the electrolyte. The implication of this effect is that very thin electrolytes will induce significant potential gradients over the electrode surfaces, as compared with a "bulk" electrolyte thickness. Hence, the corrosion or possible electrodeposition on each electrode will vary spatially over the surface. This finding is consistent with the experimental findings of Meilink et al¹¹ that indicate dendrite growth (electrodeposition) on the cathode to be more pronounced and directional and less uniform in thin electrolyte than in bulk electrolyte.

The potential results of table 2 and current density results of table 3 indicate some effects that have repercussion in the design of PWB's. Table 2 indicates virtually no effect of the relative spatial position of the anode and cathode on the extremum values of potential of each. However, table 3 shows that the extreme in current density of the anode varies significantly with relative spatial positioning of the two electrodes. This is due to the thin electrolyte causing nonuniform current density on (especially) the anode surface, although the total current from the anode must equal that of the cathode. The important effect is that locally the current density through the anode surface is greater with close electrode juxtaposition, causing locally a higher corrosion rate. The ultimate finding here is that greater separation of electrodes is desirable to minimize the corrosion rate (although the reduction reaction rate, e.g., electrodeposition, seems to be unaffected). This is similar to the phenomenon experienced in separations of galvanic couples, but for a different reason. In galvanic coupling the IR drop increases with

separation, resulting in a lesser polarization of the two electrodes; with an applied potential bias, the IR drop is fixed at the applied bias level, and the effect results from nonuniformity of the anode potential due to thin electrolyte, as described above.

The effect of potential bias on the electrochemical behavior of the copper electrodes is more pronounced. The extremum values of potential between cases of increasing bias are displayed in table 2. In table 3, the effect of varying the potential bias results in different magnitudes of variation in the extremum values of current density on the electrodes. Progressing in bias from 500 mV to 750 mV and to 1000 mV, the applied current density on the cathode increases monotonically with bias, following the cathodic branch of copper's polarization curve (figure 3A). The applied current density on the anode, however, increases between the 500 mV and 750 mV case, this describes in the 1000 mV case. This variation corresponds to the current density values around the passive peak in the anodic branch of the curve. The effect of potential bias thus depends on the shape of the polarization curve, as well as geometric effects that are minimized in this study. This result indicates no absolute general guideline for design of PWB layouts, except that a numerical analysis should be performed to assess the specific effects in each situation.

The effect of electrolyte conductivity is exhibited by cases 1A, 1D, 1E, and 1F, with results in table 2. Since the IR drop is held constant in these three cases at a bias of 500 mV, examination of Ohm's law (shown below) shows that any change in conductivity (σ) affects the overall resistance ($R \sim 1/\sigma$), i.e.,

$$\Delta\phi_{\text{bias}} = IR. \quad (1)$$

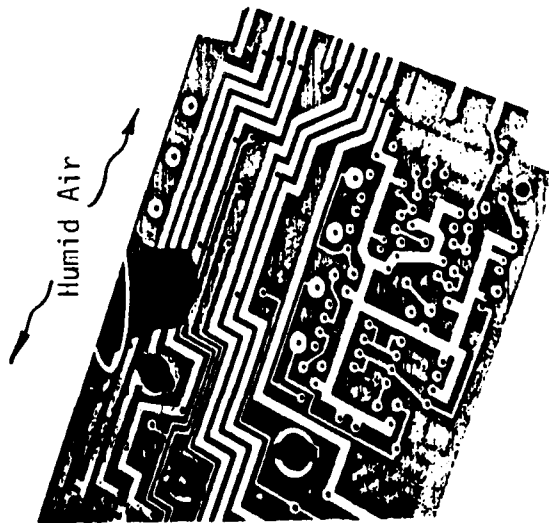
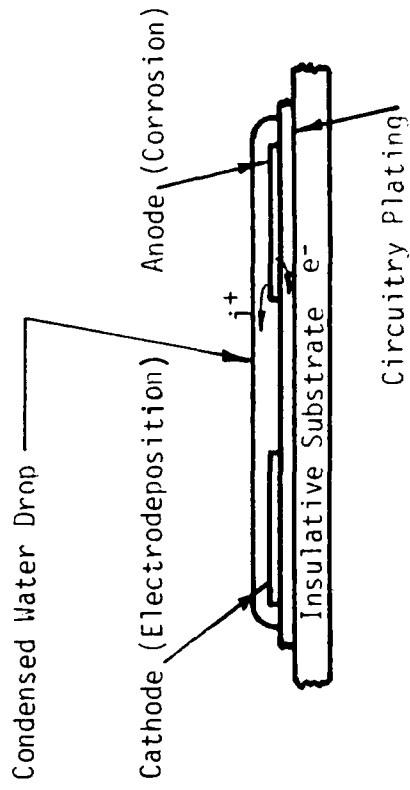
Therefore, there must be similar change in each electrode's total current, including local variations in current density (i). This latter effect explains the nonuniform current density exhibited by Case 1D in figure 5B. So, the effects of conductivity on, ultimately, corrosion at the anode and electrodeposition at the cathode are mixed. Increased conductivity appears (table 3) to decrease significantly the peak current density at the anode and slightly reduce the peak current density at the cathode. This effect might suggest that increasing the conductivity would decrease the peak local corrosion rate and therefore might be a design goal. For example, it may be advantageous to dope the PWB insulator surface with a substance that would leach into a condensed electrolyte to increase its conductivity. However, this behavior seems contrary to Ohm's Law, which would predict that for a fixed bias ($\Delta\phi$), an increase in conductivity would cause an increase in total current in both electrodes. Indeed, this is substantially what is borne out by the cathodic currents in table 3 which would indicate that the average (and thus total) current density at the anode increased concomitant with cathodic current as the conductivity increased. A further complication to this explanation is that the imposed potential bias is between the center points of each electrode. This would allow variations in potential along their surfaces consistent with nonuniform current densities.

CONCLUSIONS

The results presented in this document indicate that, using the methods of numerical corrosion analysis developed earlier, with the addition of relative boundary conditions for potential bias, the effects of atmospheric corrosion on microelectric circuits may be modeled. It is important to state that such analysis must include the complete nonlinear description of the metal/electrolyte system and must accurately account for the geometry of the electrolyte, including very thin dimensions.

The design considerations that emerge from this study are preliminary but indicate that separation distance is not as strong a mitigator of total corrosion and electrodeposition reactions for imposed potential bias situations as it is for purely galvanic situations. However, increasing separation of the electrodes results in a more uniform distribution of current density, allowing more general corrosion and electrodeposition rates. Reducing the conductivity of the electrolytes seems to have mixed effect: the total currents on the electrodes are reduced, but they are rendered less uniform, causing a more acute corrosion or electrodeposition situation on a small portion of the electrode, the latter of which would drive the dendritic growth problems reported in the literature. The almost-one-dimensional potential distribution of figure 4 suggests that, with further development, thin-electrolyte problems may be describable using 1-D analyses.

The capability described herein represents a new tool that may be applied to determine general design guidelines and to examine specific situations of geometry and metal/electrolyte combinations.



Temperature Cycling

Galvanic Situation - two different metals (e.g. Cu and Pb-Sn)
Potentiostatic Situation - same metals at different potentials

FIGURE 1 - Conditions for Atmospheric Corrosion

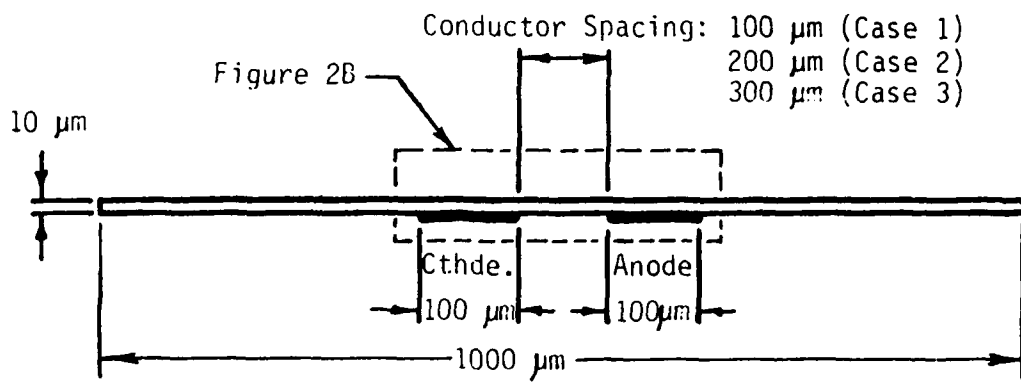


FIGURE 2A - Geometry of Electrolyte Section

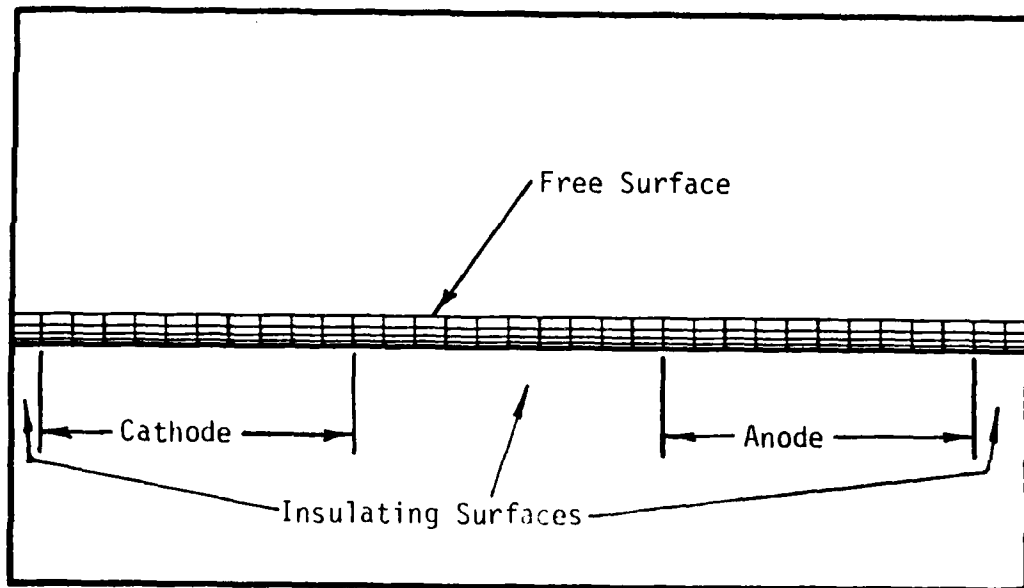


FIGURE 2B - Finite Element Model of Electrolyte

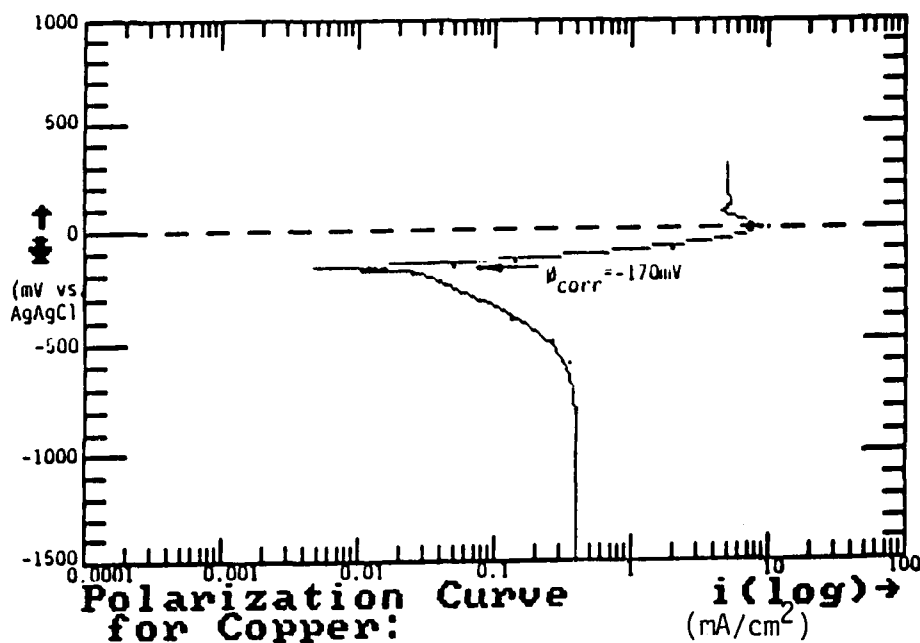


FIGURE 3A - Polarization Curve for Copper in Seawater Condensate Electrolyte

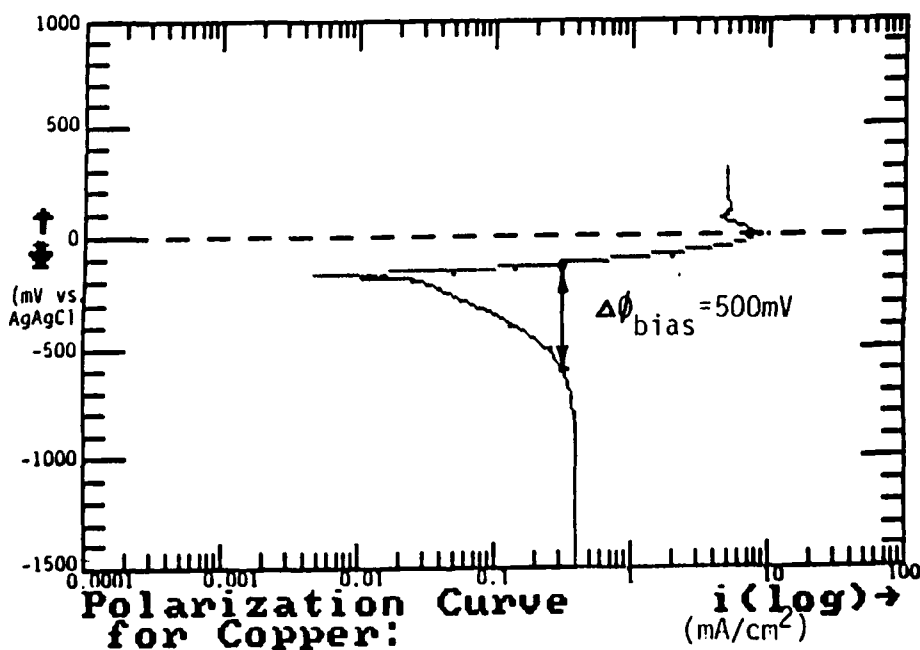
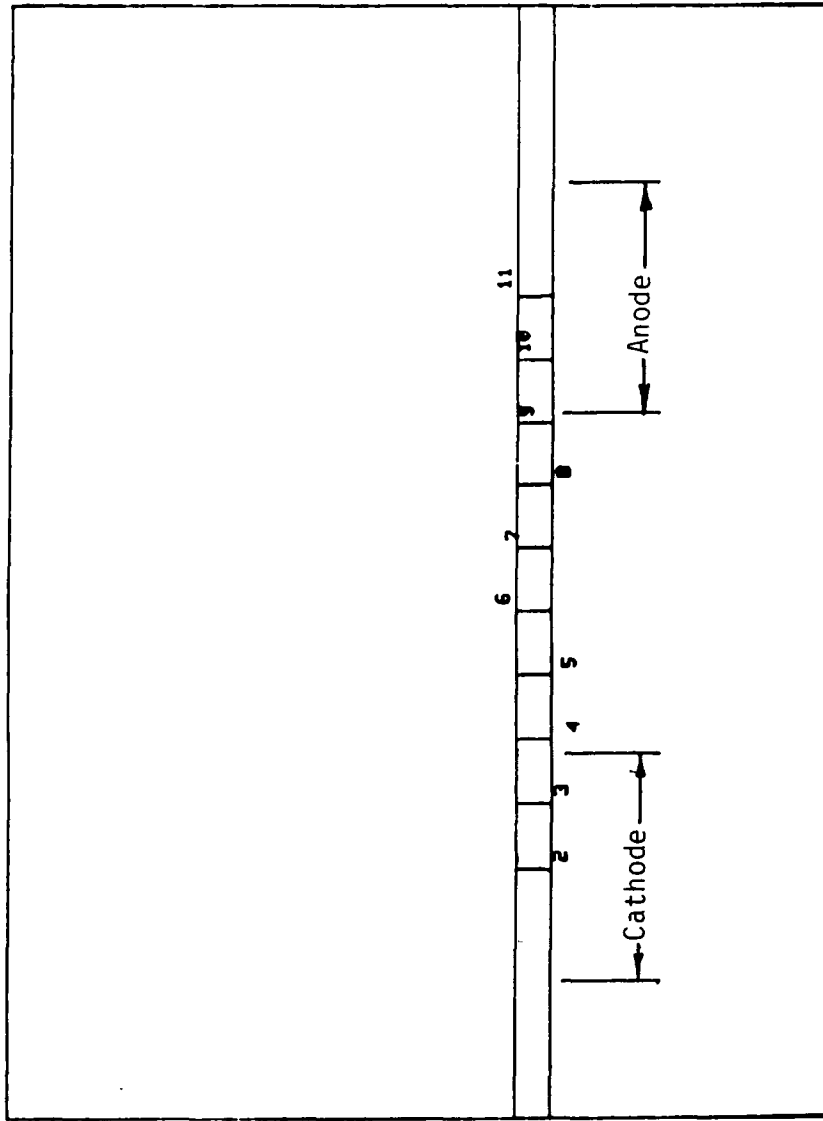


FIGURE 3B - Polarized Copper Electrodes in Seawater Condensate Electrolyte



(Contour No.) Potential (mV vs. AgAgCl)

- 1) -5.60+2
- 2) -5.150+2
- 3) -4.695+2
- 4) -4.242+2
- 5) -3.785+2
- 6) -3.335+2
- 7) -2.881+2
- 8) -2.428+2
- 9) -1.974+2
- 10) -1.520+2
- 11) -1.065+2
- 12) -6.130+1

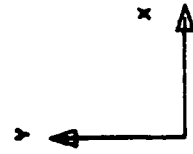


FIGURE 4 - Nearfield Distribution of Electrochemical Potential in Electrolyte

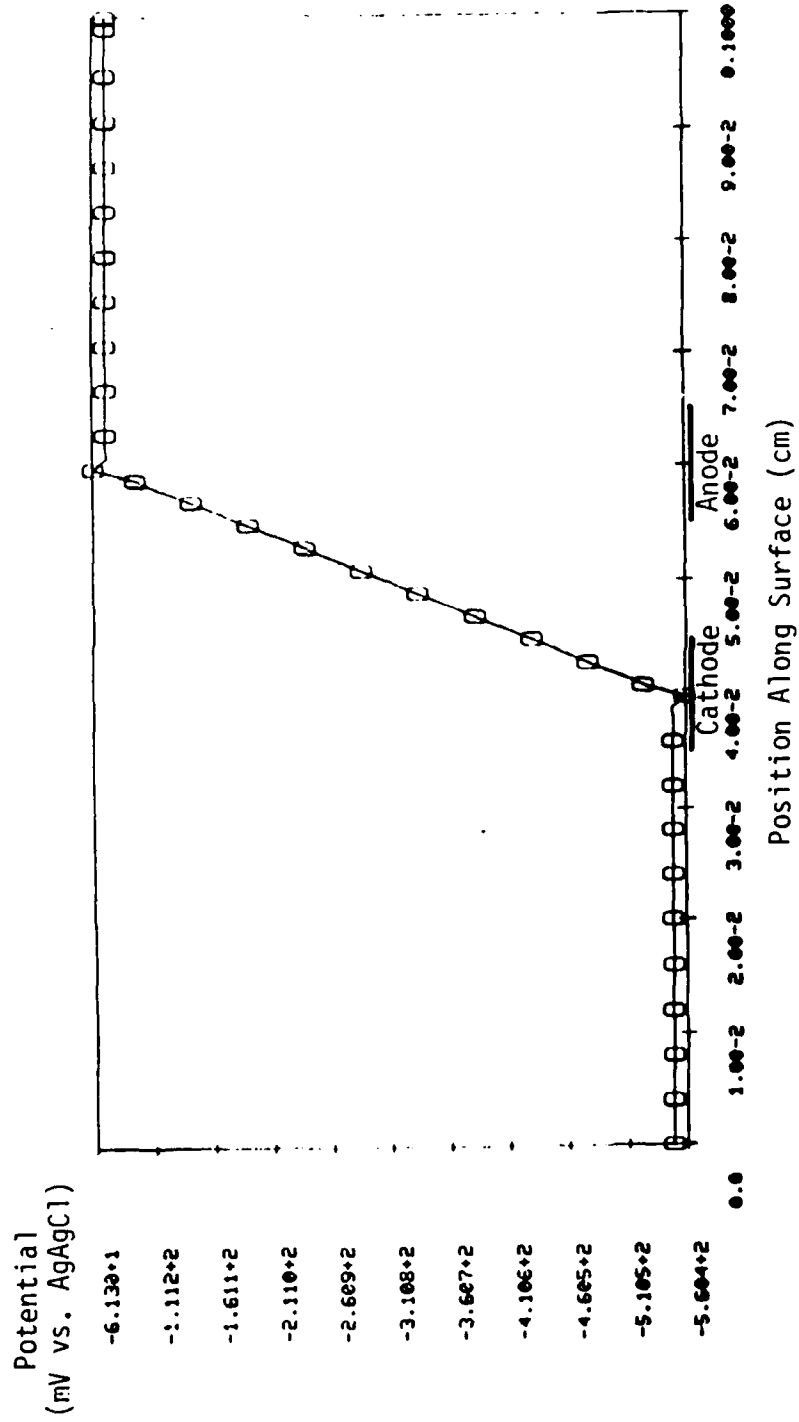


FIGURE 5A - Case 1D Potential Distribution over PWB Surface

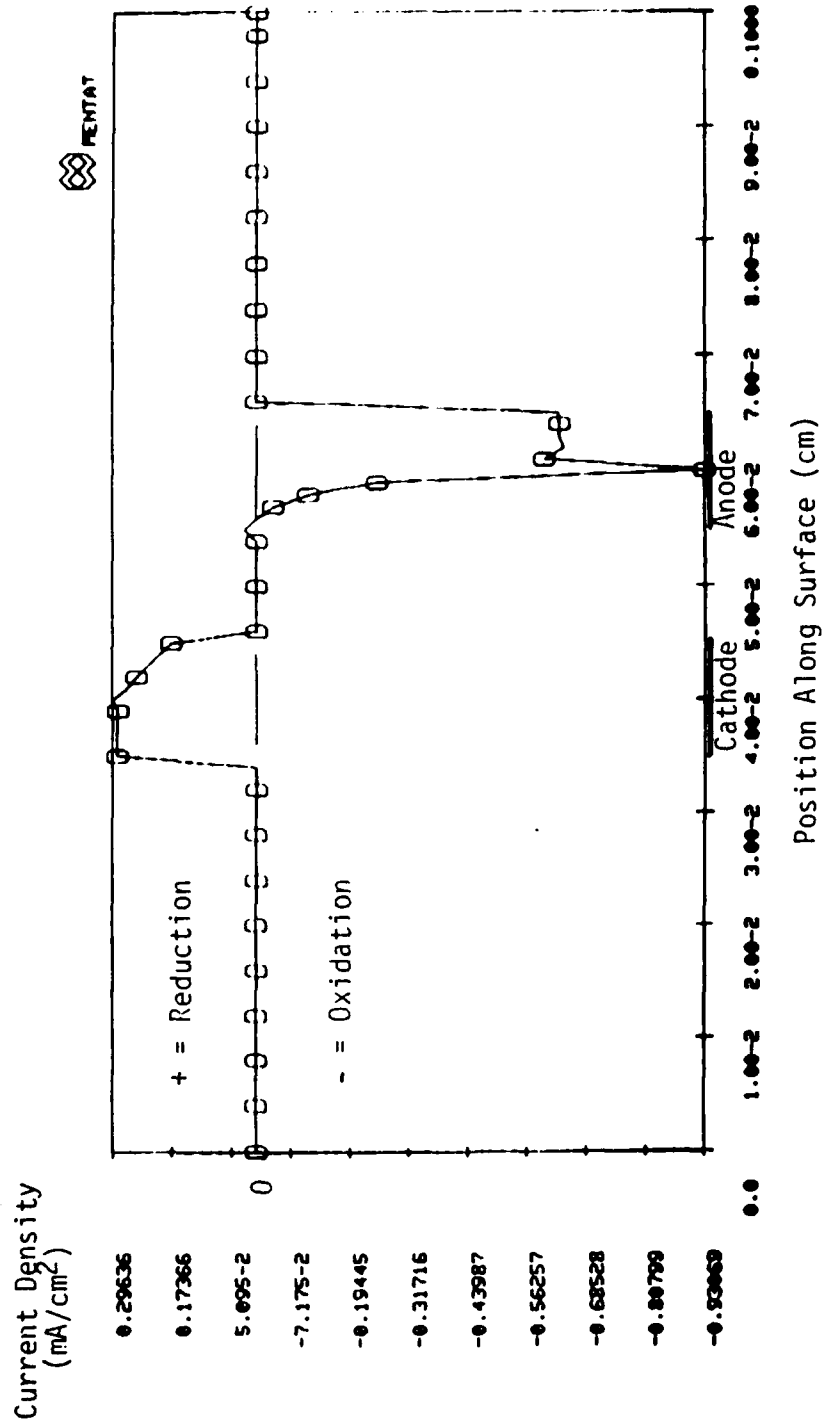


FIGURE 5B - Case 1D Current Density Distribution over PWB Surface

TABLE 1
Printed Wiring Board Analysis Cases

Bias Potential ↓	Conductor Spacing →			Electrolyte Conductivity *
	100 μm	200 μm	300 μm	
500 mV	1A	2A	3A	σ_{SW}
750 mV	1B	2B	3B	σ_{SW}
1000 mV	1C	2C	3C	σ_{SW}
500 mV	1D			$\sigma_{\text{SW}}/10$
500 mV	1E			$\sigma_{\text{SW}}/2$
500 mV	1F			$10 \cdot \sigma_{\text{SW}}$

* σ_{SW} = conductivity of seawater = 0.037 Mho/cm

TABLE 2
Potential* Results for Analysis Cases

Case Designation	1	2	3
A	-110/-609	-112/-611	-113/-612
B	+88/-660	+86/-663	+88/-662
C	+324/-674	+325/-675	+323/-675
D	-61/-560		
E	-103/-602		
F	-116/-616		

* Potentials are at Anode/Cathode, in mV vs. AgAgCl

TABLE 3
Current Density* Results of Analysis Cases

Case Designation	1	2	3
A	-0.158/+0.328	-0.146/+0.329	-0.139/+0.330
B	-7.56/+0.353	-7.40/+0.354	-6.43/+0.354
C	-5.03/+0.359	-5.04/+0.359	-5.00/+0.359
D	-0.931/+0.296		
E	-0.205/+0.324		
F	-0.121/+0.332		

* Current Densities at Anode/Cathode, in mA/cm²

REFERENCES

1. B. Dobbs, G. Slenski, Materials Performance, vol. 23, no. 3, 1984, p. 35.
2. R. S. Munn, "Electrochemical Modeling," NUSC Technical Memorandum 801018, Naval Underwater Systems Center, New London, CT, 1977.
3. R. G. Kasper, "Equivalent Electromagnetic/Acoustic Formulations Developed from the Theory of Elasticity," NUSC Technical Report 5533, Naval Underwater Systems Center, New London, CT, 9 December 1976.
4. R. S. Munn, The Modeling of Galvanic Corrosion Systems Using Numerical Methods with Particular Attention to Boundary Conditions of Nonlinear Polarization, University Microfilms International (No. 8622931), Ann Arbor, MI, 1986.
5. R. S. Munn, Materials Performance, vol. 21, no. 8, 1982, p. 29.
6. R. G. Kasper and M. G. April, Corrosion, vol. 39, no. 5, 1983.
7. R. G. Kasper and C. R. Crowe, "Comparisons of Localized Ionic Currents as Measured from 1-D and 3-D Vibrating Probes with Finite Element Predictions," ASTM G-1 Symposium Paper, Philadelphia, PA, November 1986.
8. C. R. Crowe, R. G. Kasper, and R. S. Munn, "Measurements and Numerical Analysis of Pit and Crevice Corrosion Phenomena," NACE Corrosion '87 Research Symposium Paper, Houston, TX, March 1987.
9. E. McCafferty, "Mathematical Analysis of Circular Corrosion Cells Having Unequal Polarization Parameters," NRL Report No. 8107, Naval Research Laboratory, 1977.
10. W. T. Shieh, Corrosion, vol. 40, no. 10, 1984, p. 511.
11. S. L. Meilink, M. Zamanzadeh, G. W. Warren, and P. Wynblatt, "Modeling the Failure of Electronic Devices by Dendrite Growth in Bulk and Thin Layer Electrolytes," NACE Corrosion '87 Symposium Paper No. 337, Houston, TX, March 1987.